



ELSEVIER

Available online at www.sciencedirect.com

SCIENCE @ DIRECT®

Nuclear Instruments and Methods in Physics Research B 203 (2003) 225–230

NIM B
Beam Interactions
with Materials & Atomswww.elsevier.com/locate/nimb

Trajectory-dependent energy- and charge-transfer in collisions of $\text{Br}^+(\text{}^3\text{P}_2)$ with $\text{Pt}(1\ 1\ 1)$

P.L. Maazouz, M. Maazouz, D.C. Jacobs *

Department of Chemistry and Biochemistry, University of Notre Dame, Notre Dame, IN 46556, USA

Abstract

Collisions of hyperthermal energy $\text{Br}^+(\text{}^3\text{P}_2)$ with $\text{Pt}(1\ 1\ 1)$ produces scattered $\text{Br}^-(\text{}^1\text{S}_0)$ with a yield approaching 7%. The energy distribution of the scattered product exhibits an unusual dependence on the collision energy. Specifically, as the incident energy increases from 34 to 54 eV, the peak energy of scattered $\text{Br}^-(\text{}^1\text{S}_0)$ decreases. Furthermore, the anion yield reaches a sharp maximum when $\text{Br}^+(\text{}^3\text{P}_2)$ approaches the surface with 26 eV of translational energy. The unusual scattering behavior is attributed to a trajectory dependent collision-induced deformation of the lattice. The corresponding electronic perturbation evolves synchronously with the motion of the departing projectile – leading to an enhanced charge-transfer probability.

© 2003 Elsevier Science B.V. All rights reserved.

PACS: 34.50.Dy; 34.70.+e; 79.20.Rf; 82.20.Rp

Keywords: Charge exchange; Energy exchange; Transient deformation; Ion-surface scattering; Resonance; Normal incidence

1. Introduction

The interaction of hyperthermal energy ions with solid surfaces has attracted considerable attention, because the collision energy is sufficient to activate a variety of interesting chemical processes, yet not so high as to inflict permanent damage on the surface [1]. Hyperthermal energy ions are employed in the fabrication of microelectronics devices and in the deposition of protective coatings. Notwithstanding, the fundamental dynamics leading to energy- and charge-exchange in ion/

surface collisions is not fully understood across the hyperthermal energy range.

Charge exchange at surfaces has been extensively studied for ion impact energies exceeding 1 keV [2]. The electron dynamics are often described in terms of the level shift (the alignment of the atom's affinity level relative to the Fermi level) and the level width (the strength of the electronic coupling between the atomic and surface states) [3]. Although theoretical efforts have successfully modeled charge exchange for particle/surface systems in which the lattice is assumed to be static on the time scale of the collision, few studies have treated charge exchange in the presence of a collision-induced deformation of the lattice.

Throughout the last decade, Cooper and coworkers published a series of seminal papers on the

* Corresponding author. Tel.: +1-574-631-8023; fax: +1-574-631-6652.

E-mail address: jacobs.2@nd.edu (D.C. Jacobs).

scattering, trapping and charge transfer of atomic ions at single-crystal surfaces [4]. By combining high-resolution scattering experiments with realistic classical trajectory calculations, they were able to correlate specific energy- and charge-transfer behavior with particular types of trajectories. For example, Keller et al. studied the scattering of hyperthermal energy Na^+ on $\text{Cu}(001)$ and resolved multiple peaks in the velocity distribution of the scattered projectile [5]. Their measurements of the charge fractions, corresponding to each peak within the velocity distribution, allowed them to assign the neutralization probability for various representative trajectories.

In the present study, the energy- and charge-exchange of state-selected $\text{Br}^+(^3\text{P}_2)$ on $\text{Pt}(111)$ is characterized as a function of the collision energy. The anion yield exhibits an anomalous resonance, and the corresponding energy distribution of Br^- shows a non-monotonic dependence on the incident energy. Both phenomena are explained by a collision-induced deformation of the lattice that is sensitive to the trajectory by which the incident projectile impacts the surface.

2. Experimental

The experimental apparatus has been described in detail elsewhere [6,7]. Within an ultrahigh vacuum scattering chamber, the incident Br^+ ions are formed at the intersection of a pulsed molecular beam and a pulsed ultraviolet laser. Photodissociation of Br_2 , followed by resonance-enhanced multiphoton ionization of the nascent fragments, creates Br^+ predominantly in the $^3\text{P}_2$ electronic state [8,9]. The resulting ions are accelerated by electrostatic lenses, mass-selected within a Wien filter, and decelerated to the final beam energy (11–104 eV). The packet of state-selected $\text{Br}^+(^3\text{P}_2)$ ions is directed to a clean $\text{Pt}(111)$ crystal ($T_s = 300$ K) at normal incidence. A novel imaging detector is employed to count the incident and scattered ions with mass-, angular- and velocity-resolution [10]. The detector is positioned along the ion-beam axis, where it collects ions scattered within $\pm 28^\circ$ (in-plane) and $\pm 7^\circ$ (out-of-plane) of the surface normal. A one-dimensional energy distribution

is constructed by integrating the recorded two-dimensional energy distribution over all collected angles. By integrating the one-dimensional energy distribution over all exit energies, and dividing the result by the corresponding number of incident ions, a relative yield is obtained.

3. Results and discussion

Across the translational energy range explored (11–104 eV), collisions of $\text{Br}^+(^3\text{P}_2)$ with $\text{Pt}(111)$ result in complete neutralization of the projectile as well as the emergence of Br^- . Because only Br^- in its ground electronic state, $^1\text{S}_0$, is stable against autodetachment, the scattering experiment resolves the state-to-state transformation of $\text{Br}^+(^3\text{P}_2)$ to $\text{Br}^-(^1\text{S}_0)$ on $\text{Pt}(111)$ at $T_s = 300$ K.

Fig. 1 shows a series of one-dimensional energy distributions recorded for the $\text{Br}^-(^1\text{S}_0)$ products.

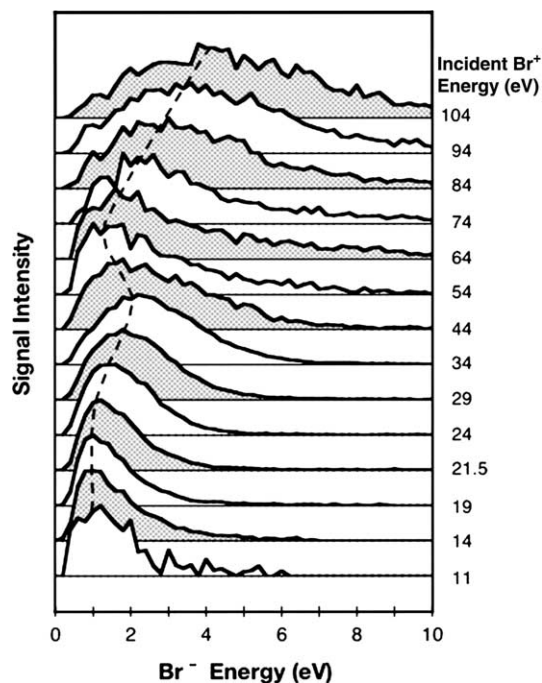


Fig. 1. A series of product $\text{Br}^-(^1\text{S}_0)$ energy distributions for various incident $\text{Br}^+(^3\text{P}_2)$ energies on $\text{Pt}(111)$. All energy distributions are rescaled to share a common peak intensity. The incident energy of the projectile is indicated next to each distribution. A dashed curve tracks the most probable exit energies.

Each distribution is measured at a different incident $\text{Br}^+(^3\text{P}_2)$ energy. The dashed curve in Fig. 1 traces the $\text{Br}^-(^1\text{S}_0)$ peak energy as a function of the incident $\text{Br}^+(^3\text{P}_2)$ energy. For impact energies between 11 and 34 eV and for those greater than 54 eV, the $\text{Br}^-(^1\text{S}_0)$ peak energy shifts to higher values as the incident energy increases. Surprisingly however, the $\text{Br}^-(^1\text{S}_0)$ peak energy *decreases* with increasing $\text{Br}^+(^3\text{P}_2)$ energy between 34 and 54 eV. This non-monotonic behavior suggests that different types of scattering trajectories dominate within distinct incident-energy regimes.

A more complete picture of the scattering behavior is shown in Fig. 2, where the logarithm of the scattering intensity is plotted against the incident $\text{Br}^+(^3\text{P}_2)$ energy and the $\text{Br}^-(^1\text{S}_0)$ exit energy. The contour diagram reveals at least two distinct scattering regimes. A resonance appears at 26 eV, and a second peak, with an order-of-magnitude less intensity, occurs near 100 eV. In between these two features, the scattering intensity diminishes sharply. As a gauge for comparison, a line is

overlaid on the contour plot to reveal the projectile energy predicted by the binary collision model (BCM). Both experimental peaks appearing within Fig. 2 lie well below the BCM prediction. This suggests that the bromine projectile does not simply scatter from a single surface atom. Moreover, if the projectile were to undergo a sequence of binary collisions, the most probable exit energy would be expected to lie above the BCM prediction [4,11]. Instead, the data suggests that the projectile simultaneously disturbs multiple surface atoms – producing a greater amount of energy loss.

The family of trajectories, leading to the resonance at 26 eV, leaves the projectile with proportionally more kinetic energy than does the family of trajectories responsible for the 100 eV feature. Many authors have previously reported that the amount of collisional energy transfer is correlated with the impact site on the surface [12–14]. For example, scattering from an atop site is non-equivalent to scattering from a three-fold hollow

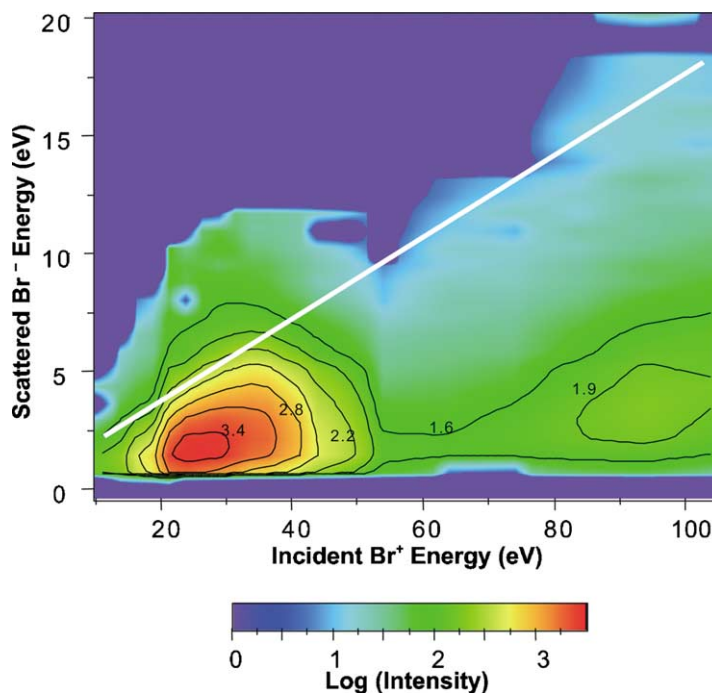


Fig. 2. Contour diagram showing the logarithm of the $\text{Br}^-(^1\text{S}_0)$ signal intensity as a function of the incident $\text{Br}^+(^3\text{P}_2)$ energy and the product exit energy. The white line represents the BCM prediction for a Br projectile undergoing a single collision with a target Pt atom (180° deflection angle).

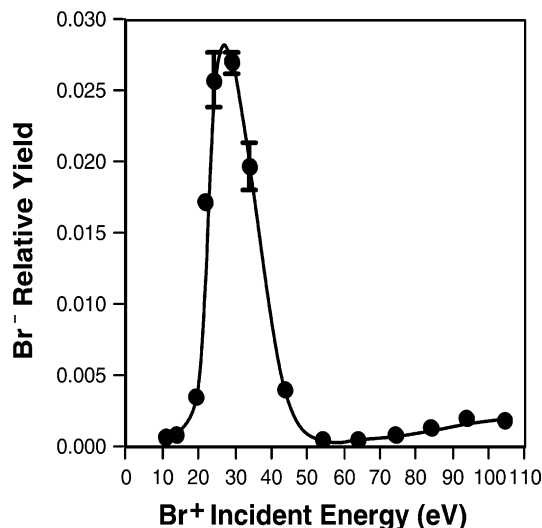


Fig. 3. Relative yield of scattered $\text{Br}^- (^1\text{S}_0)$ versus kinetic energy for $\text{Br}^+ (^3\text{P}_2)$ incident on Pt(111). The curve is drawn to guide the eye.

site or a bridge site. Furthermore, investigators have concluded that the charge-transfer probability also depends on the impact site [5,15]. The surprising result from Fig. 2 is that the preferred impact site for $\text{Br}^- (^1\text{S}_0)$ emergence varies dramatically with incident energy. To compare the product yields associated with the 26 and 100 eV features, the distributions in Fig. 2 are integrated with respect to the $\text{Br}^- (^1\text{S}_0)$ exit energy. Fig. 3 shows the relative yield of $\text{Br}^- (^1\text{S}_0)$ as a function of the incident $\text{Br}^+ (^3\text{P}_2)$ energy. The relative yield represents the fraction of incident ions that are converted into product ions and detected. This yield should not be confused with the negative ion fraction, i.e. the ratio of negative ion products to the total number of scattered products. Given the solid angle of collection for the detector and the measured angular distribution of the products, it is estimated that the total anion yield is approximately 2.5 times the relative yield reported in Fig. 3 [7]. Thus the resonance feature at 26 eV converts approximately 7% of the incident $\text{Br}^+ (^3\text{P}_2)$ ions into scattered $\text{Br}^- (^1\text{S}_0)$ products.

For $\text{Br}^+ (^3\text{P}_2)/\text{Pt}(111)$, the electron affinity (3.36 eV) [16] of the bromine projectile is less than the work function (5.95 eV) [16,17] for Pt(111). Therefore, conventional resonant charge-transfer

theory predicts that the scattered anion yield should increase monotonically with incident energy [2,18,19]. In contrast, the resonance feature, appearing in Fig. 3, exhibits a full-width half-maximum of only 15 eV. The prevailing assumption in charge-transfer models is that the lattice remains stationary on the time scale of the particle/surface interaction. However, when a heavy projectile collides at normal incidence with a surface, shock waves are produced by the violent impact [14,20,21]. In the present experiments, a 26-eV $\text{Br}^+ (^3\text{P}_2)$ projectile rapidly dumps approximately 27 eV of translational and electronic energy into a localized region of the surface.¹ The impulsive energy transfer to the surface creates a transient deformation of the lattice; an indentation forms in the first 100 fs after impact. This lattice distortion evolves on a comparable time scale as the motion of the departing projectile ($v \sim 1 \text{ \AA}/45 \text{ fs}$). The critical question remains how the surface electronic system and consequently the charge-transfer dynamics are coupled to the transient lattice deformation.

Although experiments have demonstrated significant local effects for charge transfer on alkali-covered metal surfaces, relatively few studies have investigated the influence of point defects on charge-transfer rates [22]. Static point defects on a surface (e.g. adatoms and vacancies) influence the local electron density. Silva et al. modeled the interaction of H^- and F^- with a vacancy site on Al(111) [23]. They reported that the transferred electron is repelled away from the vacancy site, thus destabilizing the atomic energy level and reducing the corresponding level width. The same group noted that an Al adatom perturbs the level shift and level width for $\text{H}^-/\text{Al}(111)$ in the opposite direction [24].

It is reasonable to expect that a transient deformation of the lattice, following a violent collision,

¹ When 26 eV $\text{Br}^+ (^3\text{P}_2)$ is incident on Pt(111), the scattered $\text{Br}^- (^1\text{S}_0)$ product leaves with only 2.1 eV kinetic energy. The asymptotic exoergicity of the double electron-transfer is calculated from the ionization potential (11.81 eV) and the electron affinity (3.36 eV) of Br minus twice the work function (5.95 eV) of Pt(111). Consequently, $\sim 27 \text{ eV}$ is deposited as both electronic and vibrational excitations in the lattice.

sion, will perturb the charge-transfer dynamics as long as the projectile does not exit too quickly [25]. Keller et al. invoked a collision-induced lattice deformation to explain the charge transfer of Na^+ on $\text{Cu}(001)$ [5]. When comparing 7.5 and 50 eV Na^+ incident on $\text{Cu}(001)$, the authors noted that two different trajectories, resulting in the same exit velocity, exhibited charge-transfer probabilities that differed by a factor of 7. The Cornell group applied a simple static dipole model to treat the collision-induced vacancy and succeeded in achieving qualitative agreement with their data.

In discussing the present experiment results, it is important to underscore that the transient surface deformation evolves on a time scale comparable to the projectile's interaction time with the surface. The synchronization of the lattice deformation with the projectile's departing trajectory generates time-dependent electronic couplings between the projectile's affinity level and the occupied states at the surface. Depending on the impact site at the surface, both the collision-induced surface deformation and the projectile's exit trajectory will be affected. The contour diagram in Fig. 2 suggests that two different impact sites contribute heavily to the overall scattering behavior. The families of trajectories resulting from collisions proximate to these two surface sites exhibit dramatically different charge-transfer probabilities.

When $\text{Br}^+(^3\text{P}_2)$ approaches the surface with 54–104 eV of kinetic energy, up to 1% of the incident ions are converted to $\text{Br}^-(^1\text{S}_0)$; the product anions leave with 5.4% of the incident energy [7]. The trajectories contributing to this scattering regime are consistent with conventional charge- and energy-transfer behavior, i.e. the anion yield grows monotonically with increasing projectile energy (See Fig. 3), and the $\text{Br}^-(^1\text{S}_0)$ energy distributions shift systematically to higher energies as the incident energy exceeds 54 eV (See Fig. 1). Consequently, there is no evidence to suggest that the impact sites, associated with this family of trajectories, form transient deformations that significantly perturb the charge-transfer dynamics as the projectile scatters from the surface.

In contrast, the trajectories connected with the 26 eV resonance exhibit anomalous energy- and charge-transfer behavior. The energy distributions

in Fig. 1 shift to higher and then lower energy as the incident energy is ramped up to 55 eV. Near the resonance, approximately 8% of the incident energy appears as kinetic energy in the scattered product [7]. Remarkably, the total anion yield approaches 7% on resonance but drops precipitously to either side of 26 eV (See Fig. 3). We propose that the strong enhancement in the anion yield near 26 eV arises from a perturbation to the local electronic structure induced by a transient deformation of the lattice [7]. The projectile's violent collision with the $\text{Pt}(111)$ surface creates an indentation in the lattice that evolves on a comparable time scale as the translation of the departing projectile. The synchronization of these two motions leads to time-dependent couplings that are phased for maximum electron transfer when 26 eV $\text{Br}^+(^3\text{P}_2)$ approaches the surface. For collision energies greater than 34 eV, the contribution of the resonance mechanism to the overall anion yield diminishes, and the energy distribution reverts to the behavior observed for scattering from other sites on the surface.

To gain additional insights into the mechanism responsible for this intriguing scattering behavior, many other studies are warranted. Molecular dynamics simulations will prove beneficial in assigning the specific impact sites and trajectories that are consistent with each scattering regime. Additionally, density functional theory calculations are needed to assess the perturbation that a surface deformation makes to the surface electronic structure and to the level-shift and level width associated with charge transfer. To test the generality of the resonance phenomena, experiments are required in which the projectile and surface are systematically varied.

Acknowledgement

Support from the National Science Foundation (CHE99-86374) is gratefully acknowledged.

References

- [1] D.C. Jacobs, *Annu. Rev. Phys. Chem.* 53 (2002) 379.
- [2] J. Los, J.J.C. Geerlings, *Phys. Rep.* 190 (1990) 133.

- [3] P. Nordlander, J.C. Tully, *Phys. Rev. B* 42 (1990) 5564.
- [4] For a comprehensive review, see B.H. Cooper, E.R. Behringer, in: J.W. Rabalais (Ed.), *Low Energy Ion–Surface Interactions, Advances in Ion Chemistry and Physics*, John Wiley & Sons, Ltd., Sussex, 1994.
- [5] C.A. Keller, C.A. DiRubio, G.A. Kimmel, B.H. Cooper, *Phys. Rev. Lett.* 75 (1995) 1654.
- [6] J.S. Martin, J.M. Greeley, J.R. Morris, B.T. Feranchak, D.C. Jacobs, *J. Chem. Phys.* 100 (1994) 6791.
- [7] M. Maazouz, P.L. Maazouz, D.C. Jacobs, *J. Chem. Phys.* 117 (2002) 10917.
- [8] Y.S. Kim, Y.-J. Jung, W. Kang, K.-H. Jung, *Bull. Korean Chem. Soc* 23 (2002) 189.
- [9] B.G. Koenders, G.J. Kuik, Karel E. Drabe, C.A. De Lange, *Chem. Phys. Lett.* 147 (1988) 310.
- [10] M. Maazouz, J.R. Morris, D.C. Jacobs, in: A. Suits, R. Continetti (Eds.), *Imaging in Chemical Dynamics*, American Chemical Society, Washington, DC, 2000.
- [11] M. Aono, *Nucl. Instr. and Meth. B* 230 (1984) 374.
- [12] E. Hulpke, K. Mann, *Surf. Sci.* 133 (1983) 171.
- [13] C.A. DiRubio, R.L. McEachern, J.G. McLean, B.H. Cooper, *Phys. Rev. B* 54 (1996) 8862.
- [14] M.C. Yang, C. Kim, H.W. Lee, H. Kang, *Surf. Sci.* 357–358 (1996) 595.
- [15] V.A. Morozov, F.W. Meyer, *Phys. Rev. Lett.* 86 (2001) 736.
- [16] D.R. Lide, *CRC Handbook of Chemistry and Physics*, eightieth ed., CRC Press, New York, 1999.
- [17] S. Link, H.A. Durr, W. Eberhardt, *Appl. Phys. A* 71 (2000) 525.
- [18] J.R. Morris, G. Kim, T.L.O. Barstis, R. Mitra, D.C. Jacobs, *J. Chem. Phys.* 107 (1997) 6448.
- [19] A. Bekkerman, B. Tsipinyuk, E. Kolodney, *J. Chem. Phys.* 116 (2002) 10447.
- [20] R. Smith, R.P. Webb, *Proc. Roy. Soc. A* 441 (1993) 495.
- [21] R. Smith, K. Beardmore, A. Gras-Marti, R. Kirchner, R.P. Webb, *Nucl. Instr. and Meth. B* 102 (1995) 211.
- [22] K.A.H. German, C.B. Weare, P.R. Varekamp, J.N. Andersen, J.A. Yarmoff, *Phys. Rev. Lett.* 70 (1993) 3510.
- [23] J.A.M.C. Silva, A.G. Borisov, J.P. Gauyacq, P. Nordlander, D. Teillet-Billy, J. Wolfgang, *Nucl. Instr. and Meth. B* 157 (1999) 55.
- [24] J.A.M.C. Silva, J. Wolfgang, A.G. Borisov, J.P. Gauyacq, P. Nordlander, D. Teillet-Billy, *Surf. Sci.* 506 (2002) 145.
- [25] J.P. Gauyacq, A.G. Borisov, *J. Phys.: Condens. Matter* 10 (1998) 6585.